AIP | Review of Scientific Instruments

A fast and accurate decoder for underwater acoustic telemetry

J. M. Ingraham, Z. D. Deng, X. Li, T. Fu, G. A. McMichael, and B. A. Trumbo

Citation: Review of Scientific Instruments **85**, 074903 (2014); doi: 10.1063/1.4891041
View online: http://dx.doi.org/10.1063/1.4891041
View Table of Contents: http://scitation.aip.org/content/aip/journal/rsi/85/7?ver=pdfcov
Published by the AIP Publishing

A fast and accurate decoder for underwater acoustic telemetry

J. M. Ingraham,[1] Z. D. Deng,[1,a)] X. Li,[1] T. Fu,[1] G. A. McMichael,[1] and B. A. Trumbo[2]
[1]*Pacific Northwest National Laboratory, P.O. Box 999, Richland, Washington 99332, USA*
[2]*U.S. Army Corps of Engineers, Walla Walla District, Walla Walla, Washington 99362, USA*

(Received 9 May 2014; accepted 12 July 2014; published online 28 July 2014)

The Juvenile Salmon Acoustic Telemetry System, developed by the U.S. Army Corps of Engineers, Portland District, has been used to monitor the survival of juvenile salmonids passing through hydroelectric facilities in the Federal Columbia River Power System. Cabled hydrophone arrays deployed at dams receive coded transmissions sent from acoustic transmitters implanted in fish. The signals' time of arrival on different hydrophones is used to track fish in 3D. In this article, a new algorithm that decodes the received transmissions is described and the results are compared to results for the previous decoding algorithm. In a laboratory environment, the new decoder was able to decode signals with lower signal strength than the previous decoder, effectively increasing decoding efficiency and range. In field testing, the new algorithm decoded significantly more signals than the previous decoder and three-dimensional tracking experiments showed that the new decoder's time-of-arrival estimates were accurate. At multiple distances from hydrophones, the new algorithm tracked more points more accurately than the previous decoder. The new algorithm was also more than 10 times faster, which is critical for real-time applications on an embedded system. © *2014 AIP Publishing LLC*. [http://dx.doi.org/10.1063/1.4891041]

I. INTRODUCTION

Several species of Pacific salmonids in the Columbia River Basin (CRB) have been listed as endangered or threatened.[1] Salmonid life history involves emigration of juveniles to the ocean, where they grow for approximately one to three years to the adult stage. As adults, salmonids migrate back upriver and return to their natal tributary to spawn.[2] In the CRB, emigrating juvenile salmonids must pass as many as eight hydropower facilities to reach the Columbia River estuary. Downstream migrating juveniles may be injured or killed while passing through the various routes (e.g., turbines, spillway, or bypass systems) at a hydropower facility.[3–8]

The U.S. Army Corps of Engineers, Portland District (Oregon, USA), developed the Juvenile Salmon Acoustic Telemetry System (JSATS) to better understand and improve fish passage and survival at federal hydropower dams.[1,8] The JSATS is capable of precise 3D tracking of fish carrying acoustic transmitters. Precision and accuracy are important when evaluating fish survival and behavior during passage through these facilities, as depth and location before passage may be influential factors in survival.[9,10] Furthermore, 3D tracking of both emigrating juvenile salmon and upriver migrating adults is useful for evaluating fish behavior as they approach and pass dams. Fish behavior coupled with route-specific survival is useful for identifying and designing structural improvements or for optimizing facility operations to enhance fish passage survival.

Underwater acoustic positioning systems have been used for oil and natural gas exploration, to monitor underwater plate tectonic movement, for underwater vehicle navigation, and to study fish behavior and survival.[11–14] The JSATS employs a series of acoustic transmitters and receivers to detect and optionally track fish in 3D. Both cabled-array and autonomous receiving systems are used to detect and decode binary-phase-shift-keyed (BPSK) tag codes sent from acoustic micro-transmitters implanted in fish. Autonomous receiving systems are deployed in open reaches of the river,[15] and cabled array systems are deployed at hydropower facilities and other locations.[14,16] Cabled array systems additionally provide the ability to gather 3D tracking data by examining the signal's time of arrival (TOA) in a real-time environment. Otherwise, the capability of autonomous system for 3D tracking is possible but not evaluated in our study. The 3D tracking algorithm requires high accuracy TOA data from a minimum of four different locations.[16] In a cabled array system, hydrophones are deployed at various fixed locations to listen for transmitted tag codes. An energy detector saves data with candidate tag codes. Finally, a decoding algorithm attempts to decode these candidate tag codes and estimates the TOA. Any improvement in the algorithm's decoding ability and TOA accuracy translates to more-accurate 3D tracks and the ability to track fish at greater distances from the hydrophones. In a recent field study, we developed a new decoding algorithm that combines greater calculation speed and accuracy with the ability to decode lower signal strengths. In this article, we describe in detail the new decoding algorithm and compare its performance to the previous algorithm.[14]

II. TRANSMISSION AND RECEPTION

Each acoustic micro-transmitter, surgically implanted in a fish, has its own unique 31-bit tag code, which consists of 7 synchronization bits, 16 tag identification (ID) bits, and 8 cyclical redundancy check (CRC) bits. A 7-bit Barker code (1110010) is used for synchronization. The tag ID is a unique binary sequence that identifies which tag sent the

a)Author to whom correspondence should be addressed. Electronic mail: zhiqun.deng@pnnl.gov

transmission. The CRC is an error detecting code that is used to remove candidate tag codes with potentially corrupted tag IDs and to reduce the false positive rate.

The tag codes are modulated onto the phase of the complex envelope of a 416.7-kHz carrier waveform. The transmitted signal, $s(t)$, is given by

$$s(t) = Re\{u(t)\exp(j2\pi f_c t)\}, \quad (1)$$

where f_c is the carrier frequency and $u(t)$ is the complex envelope:

$$u(t) = a(t)\exp[j\phi(t)]. \quad (2)$$

BPSK, the modulation scheme employed by the JSATS, represents each bit by the phase, ϕ, of the complex envelope:

when a "one" bit is being transmitted, $\phi = 0$.
when a "zero" bit is being transmitted, $\phi = \pi$.

The amplitude, $a(t)$, is constant. While a bit is being transmitted, the phase will remain constant for a period of time called the bit transmission time (T_b). The bit rate in JSATS is one-tenth of the carrier frequency, or 41.67 kilobits/s (kbps). Figure 1 shows the complex envelope of a typical JSATS tag code.

The acoustic micro-transmitters periodically broadcast their modulated tag code into the water. The frequency at which the codes are transmitted is called the pulse repetition interval (PRI). Hydrophones deployed in the water convert pressure waves into an analog signal. The JSATS receiver amplifies the analog signal and passes it through a three-pole Bessel filter with a bandwidth of 150 kHz and a center frequency of 416.7 kHz.[3] This amplified and filtered analog signal is digitized by a DSP + FPGA card (digital signal processor TMS320C6713 and field programmable gate array Xilinx XC3S1000, Innovative P25M; Innovative Integration, Simi Valley, CA, USA). The DSP + FPGA has 16 bits, a voltage range of ±2 V, and records at 2.5 megasamples/s. The DSP + FPGA employs an energy detector that searches for signals that are twice as loud as the background noise.[14] When one is found, it saves 16.384 ms (40960 samples) to a file on a local hard drive. Figure 2 shows a typical waveform saved by the energy detector. Refracted or reflected copies of a transmitted tag code often appear shortly after the line-of-sight transmission arrives. These multipath signals sometimes overlap with the line-of-sight transmission and can cause inter-symbol interference.

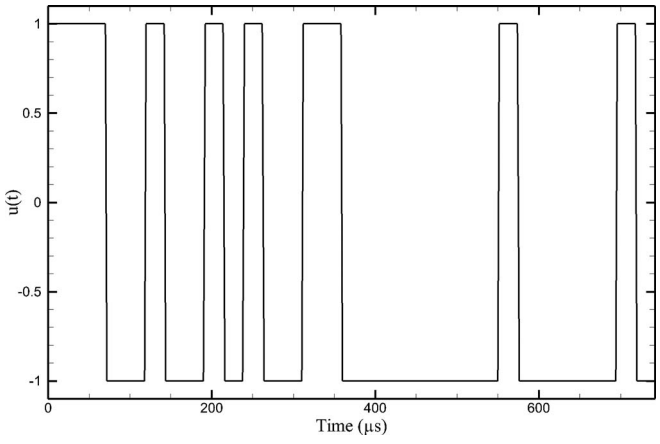

FIG. 1. Complex envelope of a typical JSATS tag code (0×72530082).

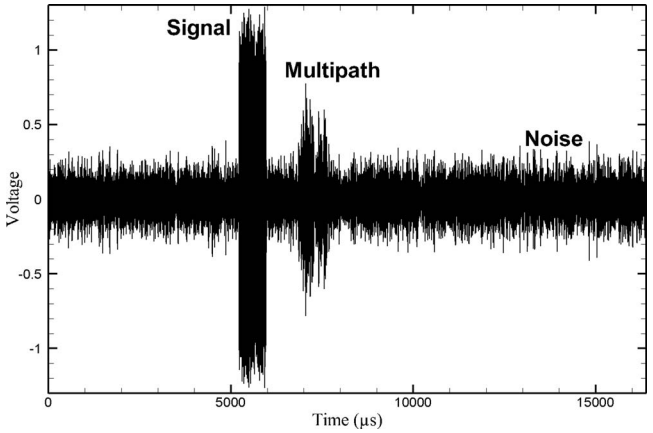

FIG. 2. An example of waveforms saved by the energy detector. Noise is present in the received data, a JSATS tag code (0×72530082) arrived at about 5200 μs, and a reflected copy of the original signal arrived at about 7000 μs.

The received digitized acoustic signal is a distorted version of the transmitted signal. The acoustic data contains noise from various sources: dam machinery, time jitter of the data sampling clock, quantization noise, self-noise of the receiving system, and thermal acoustic noise.[17] The received signal, $r(t)$, is given by

$$r(t) = Re\{v(t)\exp(j2\pi f_c t)\} + n(t), \quad (3)$$

where $v(t)$ is the complex envelope of the received signal and $n(t)$ is the noise.

The signal is further distorted by the time varying channel impulse response (CIR). The CIR includes the following: mechanical effects of the piezoelectric material in the acoustic micro-transmitter and hydrophone, signal attenuation due to geometric spreading and absorption, multipath interference caused by refraction and reflection of the signal, and distortion from the filter in the JSATS receiver. In addition, the frequency error of the acoustic micro-transmitter causes a frequency shift of the transmitter carrier wave. Finally, the received signal sampling time is not synchronized to the arrival of the transmitted signal. These effects are summarized by

$$v(t-\tau_s) = [u(t) * c(t)]\exp[j2\pi f_d(t-\tau_s) + j\phi_0], \quad (4)$$

where * denotes convolution, τ_s is the arrival time of the signal, f_d is the frequency shift, $c(t)$ is the equivalent low-pass CIR, and ϕ_0 is the phase shift of the received signal.

III. NEW DECODING ALGORITHM

A. Digital down-conversion

The new decoding algorithm attempts to decode any possible tag codes present in the saved signals. The first step is to mix the received signal from the carrier frequency to 0 Hz. Mixing, or frequency shifting, is the multiplication of an input signal by a complex sinusoid.[18] This mixed signal also contains a high frequency replica of the signal's complex envelope. The high frequency spectra can be removed by

low-pass filtering the mixed data. In addition to removing the high frequency replica, this operation removes noise and other high frequency components of the received complex envelope and allows the signal to be decimated, which reduces the computational requirements. The estimated received complex envelope of the received signal, $\hat{v}(t)$, is given by

$$\hat{v}(t) = [r(t)\exp(-j2\pi f_c t)] * h_{lp}(t), \tag{5}$$

where h_{lp} is the impulse response of the low-pass filter. All estimated parameters will have a caret over the top.

To remove the high frequency spectra and decimate the mixed signal, we use a four-stage cascaded integrator comb (CIC) filter[19] with a decimation ratio of 5, with two samples per stage and a compensating finite impulse response (CFIR) filter. The CIC filter attenuates the spectra of the high frequency replica by more than 70 decibels (dB) before it is aliased into the passband. The CIC filter's passband does not have a flat frequency response. To correct for this signal distortion, a CFIR filter was designed using the fir2 function of MATLAB®. The CFIR has an order of 256 and the impulse response is windowed with a Blackman window.[20] The combined frequency response of the CIC and CFIR is flat (±0.036 dB) from 0 to 115 kHz, and the spectrum from 125 kHz is attenuated by more than 69 dB. The CIC and CFIR filters have a linear phase response (constant group delay) that minimizes phase distortion.

B. Carrier frequency recovery

The carrier frequency of the received tag code may differ from the nominal value of 416.7 kHz by ±0.5% (2.08 kHz) due to frequency error in the acoustic micro-transmitter.[14] The carrier frequency of a BPSK signal may be found by estimating the frequency shift, first finding the peak of the Fourier transform of the input signal squared, and then dividing the peak frequency by 2.[21] The estimate is improved by only searching for peaks within the expected frequency range:

$$\hat{f}_d = \frac{1}{2} \underset{-2f_{d_{\max}} \le f \le 2f_{d_{\max}}}{\arg\max} F\{\hat{v}(t)^2\}, \tag{6}$$

where f_d is the carrier frequency shift and $f_{d_{\max}}$ is the maximum expected carrier frequency shift. The frequency shift of the signal generally still differs from the above estimate. To correct for this remaining error, 11 different carrier frequency shifts about the estimated carrier frequency shift are used in the tag code search. The frequency offsets range from −305 to 305 Hz.

C. Signal detection and phase estimation

A matched filter is the correlation of a known signal with an unknown signal to detect the presence of the known signal in the unknown signal. It can be shown that if a given input signal is passed through a filter matched to that signal, the output signal-to-noise ratio is maximized.[22] Equation (7) shows the cross-correlation, $R_{vb}(\tau)$, of the received complex envelope mixed to f_d and a template signal $b(\tau)$:

$$R_{vb}(\tau) = \overline{\hat{v}(-\tau)\exp(j2\pi \hat{f}_d \tau)} * b(\tau). \tag{7}$$

The over bar indicates complex conjugate.

The most likely phase shift of a template signal starting at a given delay is the angle of the cross-correlation, $\hat{\phi}_0(\tau)$:

$$\hat{\phi}_0(\tau) = \tan^{-1}\frac{Im\{R_{vb}(\tau)\}}{Re\{R_{vb}(\tau)\}}. \tag{8}$$

The above cross-correlation is normalized to the energy in the signals to reduce the effect that the amplitude of the envelope has on the correlation. Equation (9) calculates the correlation coefficient, $\rho_{vb}(\tau)$, by normalizing the cross-correlation to the energy of the received complex envelope and the template signal:

$$\rho_{vb}(\tau) = \frac{|R_{vb}(\tau)|}{\sqrt{E_b E_v(\tau)}}, 0 \le \rho_{vb}(\tau) \le 1, \tag{9}$$

where E_b is the energy of the template signal and $E_v(\tau)$ is the energy of the complex envelope. The energy of the template signal is constant and can be found by integrating over the length of the signal. The complex envelope's energy varies with time and contains energy that is not in phase with the transmitted signal. Only the signal energy in the complex envelope that is of the same phase as the cross-correlation is used to normalize the correlation:

$$E_v(\tau) = \int_{\tau}^{\tau+T} Re\{\hat{v}(t)\exp(j2\pi \hat{f}_d t - j\hat{\phi}_0(\tau))\}^2 dt, \tag{10}$$

where T is the time length of the template signal.

Every JSATS tag code begins with a 7-bit Barker code, which has small off-peak autocorrelation coefficients. The 7-bit Barker code is used as the known signal $b(\tau)$ in a matched filter to detect, locate, and estimate the phase of received acoustic messages. Correlation-coefficient peaks above a minimum value (e.g., 0.7) are used as the estimated arrival times ($\hat{\tau}_s$) of the transmitted JSATS tag code. In Figure 3, there is a correlation-coefficient peak of 0.95 at 5496 μs that corresponds to the arrival of the tag code.

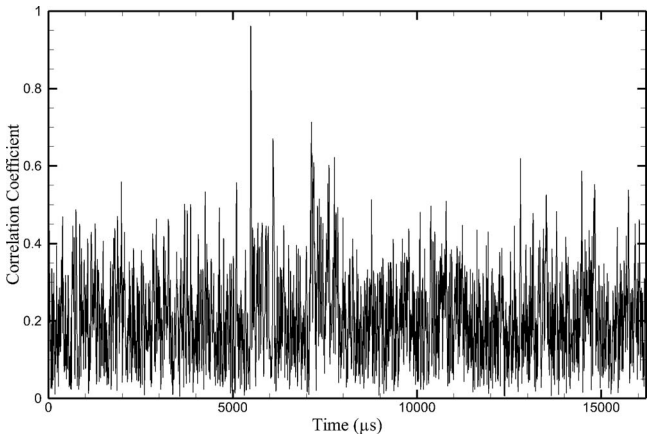

FIG. 3. Normalized cross-correlation of received complex envelope of the waveform in Figure 2 mixed to f_d and the 7-bit Barker code.

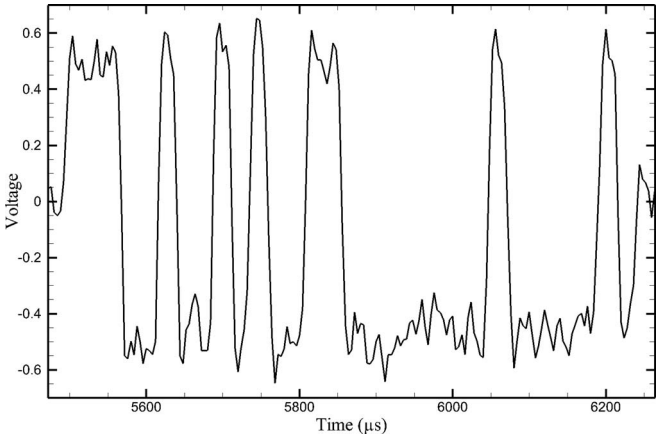

FIG. 4. Estimate of the transmitted complex envelope of the received tag code shown in Figure 2.

D. Estimated transmitted complex envelope

We can now estimate the complex envelope of the transmitted signal:

$$\hat{u}(t) = Re\{\hat{v}(t-\hat{\tau}_s)\exp(-j2\pi f_d(t-\hat{\tau}_s) - j\hat{\phi}_0(\hat{\tau}_s))\}, 0 \le t \le 31T_b. \quad (11)$$

The estimated transmitted signal still contains filtered noise, effects of the CIR, and any errors associated with the estimations of phase, start time, and carrier frequency shift (Figure 4). Excluding the effects of the CIR, the optimal filter to estimate the value of a bit would be a rectangular pulse the same length as the bit transmission time. Since the CIR acts like a low-pass filter of the received envelope, the phase shifts are not sharp. Points near phase shifts and information from prior bits can be smeared into the following bits. To minimize these effects, a rectangular pulse with a width of one-half-bit transmission time is used as the template in an additional matched filter. The filter should peak at about the center of each transmitted bit. The next peak will be T_b away. A hard decision is then made on the value of the bit. The value of the bit is 0 if $u(t) < 0$ and 1 if $u(t) > 0$.

E. Validation of tag codes

All tag codes are 31 bits. Each 31-bit combination for all 11 different starting-time offsets is checked for valid tag codes within the window being investigated. Valid tag codes start with a Barker code and have the appropriate CRC. All 31-bit combinations with the 7-bit Barker code and a valid CRC are then correlated with the complex envelope of the received data in this decoding range. The peak of this correlation is used as the start time. If the correlation-coefficient peak is above a minimum value, the tag code, its start time, its shifted frequency, and its correlation coefficient are saved to memory.

F. Multiple decodes of same tag code

After searching all carrier frequency offsets and correlation peaks, there are often multiple decodes of the same tag code. Often, the same tag code can be decoded at different frequency shifts. Refracted or reflected copies of a transmitted tag code often appear shortly after the line-of-sight transmission arrives. These multipath signals sometimes overlap with the line-of-sight transmission and can cause intersymbol interference.[22] At other times, the multipath signals arrive after the line-of-sight transmission has been received, and the decoding algorithm is able to decode the line-of-sight transmission and the copy. We only save the start time, correlation coefficient, and frequency shift of the decode that has the highest correlation coefficient within T_b of the earliest recorded start time.

G. Summary

In summary, the new decoding algorithm comprises the following steps:

1. Mix signal from 416.7 kHz to 0 Hz.
2. Apply a four-stage CIC with a decimation factor of 5 and two samples per stage.
3. Apply CFIR.
4. Decimate signal by two.
5. Estimate carrier frequency shift.
6. Mix decimated signal to estimated carrier frequency shift.
7. Find correlation coefficients of the mixed signal and the 7-bit Barker code.
8. Investigate correlation-coefficient peaks above 0.7 for valid tag codes.
9. Save codes with a 7-bit Barker code and valid CRC.

TABLE I. Comparison of the previous algorithm and the new decoding algorithm.

	Previous decoder	New decoder
Decimation	Does not decimate signal	Decimates signal by a factor of 10 for carrier frequency recovery and tag code search to improve computational efficiency; Decimates signal by 5 for TOA estimation with temporal resolution
Carrier frequency recovery	Uses 21 predefined carrier frequencies based on the expected received carrier frequency	Calculates an estimate of the carrier frequency shift based upon the input data and the expected received carrier frequency
Signal detection	Searches for energy peaks above background noise	Searches for normalized cross-correlation peaks of Barker code and signal above a minimum correlation coefficient value
Phase estimation	Uses the phase of the prior bit to estimate the value of the current bit	Uses the 7 bits in the Barker code to estimate the phase of the signal
Time of arrival	Uses the peak of the Barker code correlated with the phase of the signal as the TOA	Uses the peak of the normalized correlation of the tag code with the complex envelope of the signal to estimate the TOA

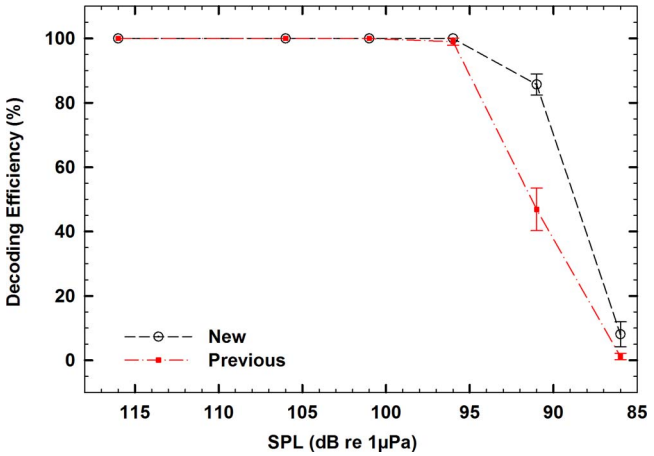

FIG. 5. Sound pressure level (SPL) versus decoding efficiency for a hydrophone mounted in the laboratory tank. Error bars represent 95% confidence interval.

10. Mix undecimated data after CFIR to estimated carrier frequency; find correlation coefficient of data and tag codes. The undecimated data after the CFIR is used for increased temporal resolution.
11. Find peak, and if it is above 0.7, save tag code and start time.
12. Repeat steps 6–12 for all the different carrier frequency offsets about the estimated carrier frequency shift.
13. Use the start time with the highest correlation coefficient that is within T_b of the earliest recorded start time.

H. Comparison with previous algorithm

The new decoding algorithm differs from the previous algorithm in several key ways. Table I summarizes these differences.

IV. RESULTS

A. Lab testing results

We performed initial laboratory testing using an acoustic transmitter and receiver setup inside a tank lined with anechoic material.[23] The anechoic material helps minimize signal reflections and multipath interference. Two tag codes were randomly selected from each group of tag codes having the same number of bit transitions, for a total of 28 tag codes. A broadband spherical hydrophone (Model TC 4034, RESON, Slangerup, Denmark) transmitted each tag code 15 times at six sound pressure levels (SPLs): 116, 106, 101, 96, 91, and 86 dB re 1 micropascal (μPa). The receiving hydrophone was placed tip-down inside the tank 1 m from the transmitter. The received waveforms were saved on a local computer and then processed with both the previous and new decoding algorithms.

Decoding efficiency is defined as the number of correct decodes divided by the number of transmissions. Each point in Figure 5 represents the mean decoding efficiency of 28 tag codes. The 95% confidence intervals of decoding efficiency from the tests are also presented in Figure 5 using error bars. The decoding efficiency of the new algorithm tailed off at a slower rate. At an SPL of 91 dB re 1 μPa, the decoding efficiency of the new algorithm was 1.8 times higher than that of the previous algorithm. For signals above 96 dB re 1 μPa, decoding efficiencies of all the 28 tag codes were 100% consistently without variation for the new decoder. 100% constant decoding efficiency could only be kept for signals above 101 dB re 1 μPa for the pervious decoder.

B. Field results and 3D tracking

In 2013, a JSATS cabled array system with 33 hydrophones was deployed at Little Goose Dam to study fish passage. Little Goose Dam opened in 1970 and spans the Snake River in Washington, ~113 km from the confluence of the Snake River and the Columbia River. Two hydrophones were installed at two different elevations at each main pier nose throughout the dam (Figure 6). To block loud noises generated by dam machinery and flow through the dam, the hydrophones were baffled by plastic cones lined with an anechoic material.[16] The position of each hydrophone was known within 5 cm.

The coordinates of the easting and northing system used to survey with hydrophones and to position dam structures were rotated clockwise to form a local dam-face sound-source tracking coordinate system (Figures 6 and 7). The tracking coordinate system x-axis is perpendicular to the dam and looks straight into the forebay; the y-axis runs along the dam face from south to north; and the z-axis is vertical, pointing upward from the bottom of the forebay to the water surface. The origin is set at normal pool surface elevation near the south end of the powerhouse.

On 19 and 20 March 2013, tests were conducted to assess the accuracy of the deployed hydrophone array and

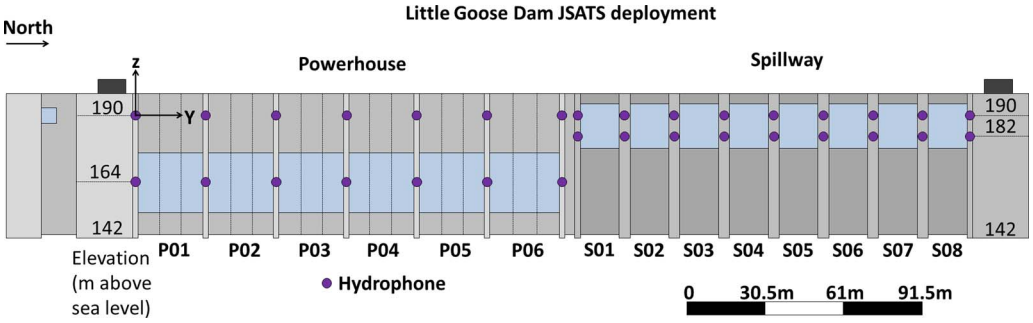

FIG. 6. Location of hydrophones and beacons deployed in the Little Goose Dam forebay.

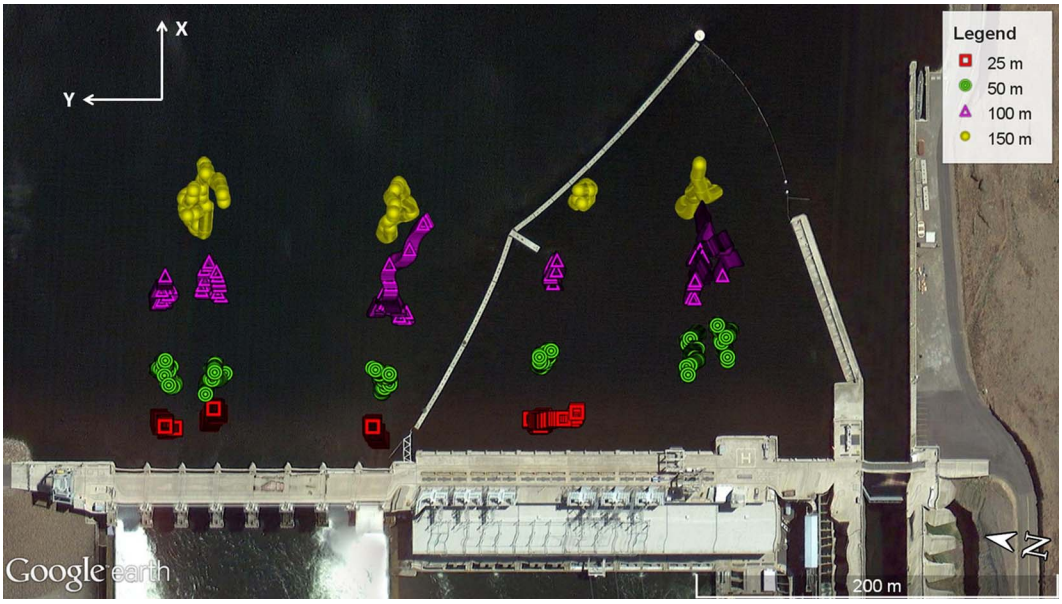

FIG. 7. GPS locations of the remote-controlled boat during stationary point testing at Little Goose Dam.

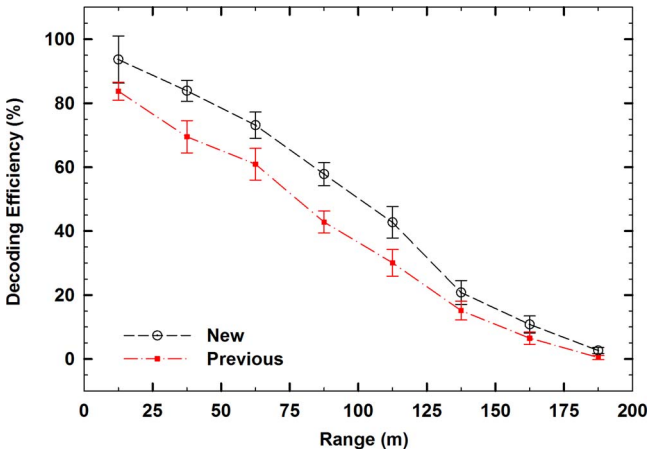

FIG. 8. Decoding efficiency of two JSATS tags versus distance at Little Goose Dam during the stationary point testing. Error bars represent 95% confidence interval.

validate tracking solvers. A remote-controlled boat with a Trimble® Geoexplorer® Global Positioning System (GPS) receiver moved to various fixed locations in the Little Goose Dam forebay (Figure 7). The GPS data was post-processed with estimated horizontal precision of 0.15 m and vertical precision of 0.17 m during the tests. Averaged PDOP value is 1.4 with a standard deviation of 0.17, while mean HDOP value is 0.73. Two JSATS tags (manufactured by Advanced Telemetry Systems, Inc., Isanti, MN), with source levels of 156 dB re 1 μPa and a 3–s PRI were mounted to the remote-controlled boat 2.25 m below the water surface. The orientations of the tags could not be controlled.

The data recorded by each hydrophone's energy detector was processed with both the previous and new decoding algorithms. Decodes of the same tag code with a time gap less than 0.3 s were considered a multipath signal and only the first arriving decodes of each transmission were kept.

TABLE II. 3D tracking efficiency, rms errors, and median errors of two JSATS tags at various stationary points in the Little Goose Dam forebay. P value is calculated from the two-sample *t*-test.

Distance		25 m		50 m		100 m		150 m	
Decoder		New	Previous	New	Previous	New	Previous	New	Previous
Efficiency (%)		97.34	96.63	90.95	88.02	54.51	43.90	23.80	14.01
Distance error	RMS (m)	0.78	1.03	1.28	1.45	1.73	4.45	3.92	7.04
	Median (m)	0.68	0.67	0.95	0.97	0.94	1.09	1.23	1.89
	P value		0.084		0.019		0.068		0.018
x error	RMS (m)	0.30	0.63	0.57	0.76	1.16	4.18	3.32	6.40
	Median (m)	− 0.06	− 0.06	− 0.18	− 0.11	− 0.35	− 0.26	0.03	0.19
	P value		0.192		0.188		0.497		0.739
y error	RMS (m)	0.37	0.51	0.71	0.75	0.89	0.91	1.95	1.64
	Median (m)	0.24	0.25	0.34	0.35	0.30	0.32	0.13	0.13
	P value		0.578		0.782		0.595		0.714
z error	RMS (m)	0.62	0.62	0.90	0.98	0.92	1.22	0.71	2.42
	Median (m)	− 0.51	− 0.48	− 0.56	− 0.59	− 0.49	− 0.46	0.05	− 0.09
	P value		0.200		0.972		0.336		0.019

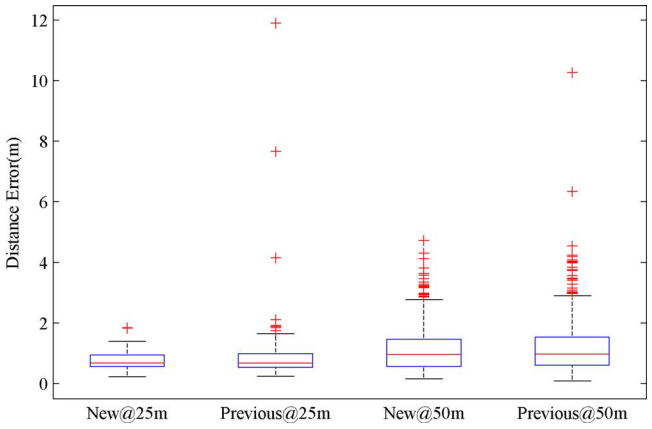

FIG. 9. Box plot of the distance error of the JSATS tags. The center line in each box indicates the median value, the edges of the box are the 25th and 75th percentiles, and the whiskers extend to the most extreme values corresponding to ~99.3% coverage without outliers, which are displayed individually by crosses.

The distance between the transmitter and the hydrophone that recorded the transmission was calculated from the TOA and the GPS position of the remote-controlled boat. For each of the two JSATS tags, the decodes at the receiving hydrophone array at LGS dam face were continuously recorded at each hydrophone. The decoding efficiency was calculated for eight different range bins from 0 to 200 m and each decode was placed into a range bin with a width of 25 m (Figure 8). For example, range = 12.5 m is indicating a horizontal range of 0-25 m (x direction). The number of transmissions in each range was estimated by dividing the PRI of the tag by the amount of time the transmitter was in that range. In Figure 8, corresponding to each range bin, the decoding efficiency was equal to averaged value of the two tags from 32 hydrophones.

Unlike the laboratory measurements, the received signals may be significantly distorted by the CIR. The new algorithm was better able to process these signals and had a higher decoding efficiency at all distances. The decoding efficiencies were much lower than they typically are in the summer because of the increased signal attenuation due to low temperature effects. The temperature in the Little Goose Dam forebay was less than 6 °C during the testing period.[24] The signal attenuation due to absorption[25] was significantly higher than when the water is 20 °C, a typical summer temperature.

An independently developed 3D tracking software from Pacific Northwest National laboratory was used to process decodes in the purpose of comparing the time accuracy of the decoding algorithms. The tracking efficiency—the number of successful 3D-tracked locations divided by the estimated number of transmissions—of JSATS tags was high for both algorithms when tracking stationary points less than 50 m away. For stationary points beyond 100 m, the new algorithm was able to track significantly more points. The distance error is the difference in distance between the transmitter location estimated from the GPS position coordinates from the remotely controlled boat and the transmitter location estimated using the solver. The errors were also calculated, respectively, in x, y, and z coordinates as differences between solver-tracked and GPS-measured values. The root-mean-square (rms) distance error was lower for the tracks made with the new algorithm at all stationary points. The median errors were about the same at distances of less than 50 m. For stationary points beyond 100 m, the median errors of the previous algorithm were 0.15 m higher (Table II). At the maximum test range of 150 m, lower SNRs caused by propagation loss of tag signals and increased opportunity for multipath may have reduced tag signal detection rates at receiving hydrophones, and introduced larger tracking errors.

TABLE III. Comparison of the time for each decoder to process 7000 files containing two channels with 16.384 ms of data.

	Time to execute (s)		Time per file (ms)		
Trial	New	Previous	New	Previous	Ratio
1	31.7	549.2	4.53	78.45	17.34
2	31.7	553.3	4.53	79.05	17.47
3	31.7	553.3	4.53	79.05	17.47
4	31.7	549.9	4.53	78.55	17.36
Mean	31.7	551.4	4.53	78.77	17.41

At different distances, the median values of the errors from new and previous decoders were similar. P values also reflected that the errors of tracking using new and previous decoders were not significantly different at a significance level of 0.05 for distance within 100 m. However, the box plot of results within the range of 25 m and 50 m in Figure 9 shows that the new algorithm improved the tracked points with less outliers, especially extreme outliers, leading to smaller RMS errors.

C. Speed

The new decoding algorithm was implemented in the C programming language and compiled with the GNU C Compiler. Seven-thousand files collected at Little Goose Dam were processed four times by each decoder on a Dell™ computer with two Intel® Xeon® X5650 processors and 24 gigabytes of RAM. Each file contains two channels with 16.38 ms of data. Both decoders are single-threaded command line programs. The execution times of both algorithms were recorded. The new algorithm was able to process 32.77 ms of data in only 4.53 ms—more than 17 times faster than the previous algorithm (Table III). The p-value calculated from the two sample t-test between trails of time cost per file using new and precious decoder was extremely small ($<10^{-6}$), indicating a significant difference between speed of new and precious decoder.

V. CONCLUSIONS

A new algorithm to decode the 31-bit BPSK signal used in the JSATS was described in detail. Laboratory and field testing showed the new algorithm was able to decode more signals than the previous algorithm. The algorithm is fast enough to run in real time on an embedded system. The techniques presented in this paper can be applied to other underwater acoustic positioning systems. The new algorithm can

be used to gather more data and more-accurate information about salmon behavior and survival and provide insight into design and operations at hydropower facilities to enhance fish passage and survival. Three-dimensional tracking data with greater accuracy and precision may also simplify identification of specific facility configurations and operation modifications for safer fish passage. Furthermore, fish passage research may experience cost efficiencies provided by the new algorithm due to decreased data processing time and smaller sample size requirements to achieve the desired data precision and accuracy.

ACKNOWLEDGMENTS

This research was funded by the U.S. Army Corps of Engineers (USACE). We greatly appreciate the assistance of USACE staff members including Martin Ahmann, Brad Eppard, Derek Fryer, Mike Langeslay, Steve Juhnke, Marvin Shutters, and Jon Renholds. Critical assistance also was provided by many staff members of the Pacific Northwest National Laboratory, including Ki Won Jung, Jun Lu, Jayson Martinez, Mitchell Myjak, Mark Weiland, and Maura Zimmerschied.

[1]W. Nehlsen, J. E. Williams, and J. A. Lichatowich, "Pacific salmon at the crossroads: Stocks at risk from California, Oregon, Idaho, and Washington," Fisheries **16**, 4 (1991).
[2]B. J. Burke, W. T. Peterson, B. R. Beckman, C. Morgan, E. A. Daly, and M. Litz, "Multivariate models of adult Pacific salmon returns," PloS One **8**(1), e54134 (2013).
[3]G. F. Cada, "The development of advanced hydroelectric turbines to improve fish passage survival," Fisheries **26**, 14 (2001).
[4]M. Odeh and G. Sommers, "New design concepts for fish friendly turbines," Int. J. Hydropower Dams **7**, 64 (2000).
[5]D. A. Neitzel, D. D. Dauble, G. F. Cada, M. C. Richmond, G. R. Guensch, R. P. Mueller, C. S. Abernethy, and B. G. Amidan, "Survival estimates for juvenile fish subjected to a laboratory-generated shear environment," Trans. Am. Fish. Soc. **133**, 447 (2004).
[6]Z. Deng, G. R. Guensch, C. A. McKinstry, R. P. Mueller, D. D. Dauble, and M. C. Richmond, "Evaluation of fish-injury mechanisms during exposure to turbulent shear flow," Can. J. Fish. Aquat. Sci. **62**, 1513 (2005).
[7]Z. Q. Deng, T. J. Carlson, G. R. Ploskey, M. C. Richmond, and D. D. Dauble, "Evaluation of blade-strike models for estimating the biological performance of Kaplan turbines," Ecol. Model. **208**, 165 (2007).
[8]G. A. McMichael, M. B. Eppard, T. J. Carlson, J. A. Carter, B. D. Ebberts, R. S. Brown, M. A. Weiland, G. R. Ploskey, R. A. Harnish, and Z. Deng, "The juvenile salmon acoustic telemetry system: A new tool," Fisheries **35**, 9 (2010).
[9]C. C. Coutant and R. R. Whitney, "Fish behavior in relation to passage through hydropower turbines: A review," Trans. Am. Fish. Soc. **129**, 351 (2000).
[10]Z. Deng, T. J. Carlson, J. P. Duncan, M. C. Richmond, and D. D. Dauble, "Use of an autonomous sensor to evaluate the biological performance of the advanced turbine at Wanapum dam," J. Renewable. Sustain. Energ. **2**(1) 053104 (2010).
[11]R. D. Christ and R. L. Wernli, *The ROV Manual* (Elsevier, San Francisco, 2014), pp. 425–426.
[12]F. N. Spiess, C. D. Chadwell, J. A. Hildebrand, L. E. Young, G. H. Purcell, and H. Dragert, "Precise GPS/acoustic positioning of seafloor reference points for tectonic studies," Phys. Earth Planet. Int. **108**, 101 (1998).
[13]N. H. Kussat, C. D. Chadwell, and R. Zimmerman, "Absolute positioning of an autonomous underwater vehicle using GPS and acoustic measurements," IEEE J. Ocean. Eng. **30**, 153 (2005).
[14]M. A. Weiland, Z. Deng, T. A. Seim, B. L. Lamarche, E. Y. Choi, T. Fu, T. J. Carlson, A. I. Thronas, and M. B. Eppard, "A cabled acoustic telemetry system for detecting and tracking juvenile salmon: Part 1. Engineering design and instrumentation," Sensors **11**, 5645 (2011).
[15]P. S. Titzler, G. A. McMichael, and J. A. Carter, "Autonomous acoustic receiver deployment and mooring techniques for use in large rivers and estuaries," North Am. J. Fisher. Manag. **30**, 853 (2010).
[16]Z. Deng, M. A. Weiland, T. Fu, T. A. Seim, B. L. Lamarche, E. Y. Choi, T. J. Carlson, and M. B. Eppard, "A cabled acoustic telemetry system for detecting and tracking juvenile salmon: Part 2. Three-dimensional tracking and passage outcomes," Sensors **11**, 5661 (2011).
[17]L. E. Kinsler, A. R. Frey, A. B. Coppens, and J. V. Sanders, *Fundamentals of Acoustics* (Wiley, New York, 1982), p. 411.
[18]M. Borgerding, "Turning overlap-save into a multiband mixing, downsampling filter bank," IEEE Signal Process. Mag. **23**, 158 (2006).
[19]E. Hogenauer, "An economical class of digital filters for decimation and interpolation," IEEE. Trans. Acoust., Speech Signal Proc. **29**, 155 (1981).
[20]A. V. Oppenheim, R. W. Schafer, and J. R. Buck, *Discrete-Time Signal Processing* (Prentice Hall, Upper Saddle River, New Jersey, 1999), pp. 468–471.
[21]J. Feigin, *Practical Costas Loop Design* (PDF), RF Design, Electronic Design Group (2002), Retrieved 2014-02-19, Also available at: http://defenseelectronicsmag.com/site-files/defenseelectronicsmag.com/files/archive/rfdesign.com/images/archive/0102Feigin20.pdf
[22]A. Goldsmith, *Wireless Communications* (Cambridge University Press, 2005).
[23]Z. Deng, M. A. Weiland, T. J. Carlson, and M. B. Eppard, "Design and instrumentation of a measurement and calibration system for an acoustic telemetry system," Sensors **10**, 3090 (2010).
[24]Columbia River DART (Data Access in Real Time), Columbia Basin Research, University of Washington, 2014, also available at http://www.cbr.washington.edu/dart/query/river_graph_text.
[25]M. A. Ainslie and J. G. McColm, "A simplified formula for viscous and chemical absorption in sea water," J. Acoust. Soc. Am. **103**, 1671 (1998).